New single particle basis for microscopic description of decay processes

D. S. Delion
Institute of Atomic Physics, Bucharest Măgurele, P.O. Box MG-6, Romania

A. Insolia
Department of Physics, University of Catania and Istituto Nazionale di Fisica Nucleare, I-95129 Catania, Italy

R. J. Liotta
KTH, Physics at Frescati, Frescativägen 24, S-10405 Stockholm, Sweden
(Received 26 May 1995)

A single particle basis consisting of two different harmonic oscillator representations is introduced with the aim of studying microscopically α- and cluster-decay processes. A correct description of the wave functions at large distances is obtained within a minimal single particle basis. Experimental data corresponding to a large number of α decay transitions from even-even nuclei are well reproduced. [S0556-2813(96)01406-9]

PACS number(s): 21.60.Gx, 23.60.+e

I. INTRODUCTION

Microscopic calculations have shown that the continuum part of the nuclear spectrum plays an important role in α-decay processes [1–4]. In particular, one needs to include the continuum, or high lying configurations in bound representations, to ensure a proper asymptotic behaviour of the α-particle formation amplitude at large distances. This is in sharp contrast to the usual spectroscopic calculations, where shell-model representations that include only a few bound states of a realistic Woods-Saxon potential are enough to describe low energy properties well [5–8]. Spectroscopic properties of well deformed nuclei could also be conveniently studied assuming that the core is a realistic Woods-Saxon potential. However, the diagonalization of such a potential is usually performed within a spherical harmonic oscillator basis, and this also requires the introduction of high lying configurations [9–12]. In the calculation of absolute decay widths this is even more important, in spherical [13] as well as in deformed nuclei [14–16]. For instance, in Ref. [1] it was found that the inclusion of 13 major harmonic oscillator shells was not enough to explain the ground-state to ground-state α-decay width of ^{212}Po. In deformed nuclei it was possible to reproduce the total α-decay width within a factor of 3, but only after including 18 major shells [15,16]. In heavy cluster decay the use of a very large number of shells in the basis improves the calculation but still the calculated absolute decay widths are too small by $2-3$ orders of magnitude with respect to the corresponding experimental data [16,17].

All these facts indicate that the description of cluster-decay processes (including α particles) within standard harmonic oscillator representations, i.e., in terms of the eigenstates of a harmonic oscillator potential with parameters just suited to the nucleus under study, is inadequate to guide experimental searches, or even reproduce experimental data [18]. Yet this is important particularly in relation to present experimental facilities and methods that would allow one to detect even tiny signals which may correspond to the decay of highly hindered processes, such as the decay of heavy clusters or very unstable states [19,20], where very high lying configurations may play an important role.

The aim of this paper is to present a single particle representation which is rather small but at the same time is adequate to describe the quasicontinuum. The basis consists of the eigenstates of two different sets of harmonic oscillator states. One is suited to describe the discrete part of the spectrum and the other one the quasicontinuum. Since the problem outlined above lies in the poor description of the decay process at large distances, i.e., deficient or incomplete high lying configurations in the basis used in the calculations, we hope that the introduction of such a representation will cure those shortcomings while the calculation itself remains feasible.

The basis becomes nonorthogonal, but the problem of dealing with a Hermitian Hamiltonian can be solved rather easily by using an orthogonalization procedure.

The formalism is described in Sec. II, applications concerning α decay processes from even-even nuclei are performed in Sec. III, and the conclusions are drawn in Sec. IV. Details about the orthogonalization procedure are given in the Appendix.

II. FORMALISM

A. The basis

The many-body problem in nuclear physics can conveniently be treated using harmonic oscillator representations. With this in mind, we write the stationary Schrödinger equation describing the single particle motion of a particle of mass M_0 in a spherical mean field $V(r)$ as

$$H\psi(\xi)\equiv\left[-\frac{\hbar\omega}{2\lambda_0}\vec{\nabla}^2+V(r)\right]\psi(\xi)=E\psi(\xi) \qquad (2.1)$$

where $\xi=(\vec{r},s)$ is the set of spatial and spin coordinates, and

$$\lambda_0=\frac{M_0\omega}{\hbar} \qquad (2.2)$$

is the harmonic oscillator parameter that best suits the potential $V(r)$ within the nuclear volume, i.e., with $\hbar\omega = 41A^{-1/3}$.

The wave function that solves the eigenvalue problem (2.1) has a separable form, i.e.,

$$\psi_{Elj\Omega}(\xi) = u_{Elj}(r)[i^l Y_l(\hat{r})\chi_{1/2}(s)]_{j\Omega} \tag{2.3}$$

where l is the angular momentum of the particle, j its total spin, and Ω the corresponding projection on the z axis. The radial part of the wave function satisfies the equation

$$-\frac{\hbar\omega}{2\lambda_0}\left[\frac{1}{r}\frac{d^2}{dr^2}r - \frac{l(l+1)}{r^2}\right]u_{Elj}(r) \equiv H_{lj}^{(\lambda_0)}u_{Elj}(r) = [E - V(r)]u_{Elj}(r). \tag{2.4}$$

The radial wave functions u_α, where α labels the set of quantum numbers $\{E,l,j\}$, are usually expanded in a harmonic oscillator (HO) basis, i.e.,

$$u_\alpha(r) = \sum_{n=0}^{\infty} c_{\alpha n} R_{nl}^{(\lambda)}(r) \tag{2.5}$$

where R_{nl}^{λ} is the HO radial wave function with radial quantum number n and angular momentum l. The HO parameter λ determines the representation. It may be convenient to choose it according to the number of shells that one includes in the basis and, therefore, it might differ from the value of λ_0 given in (2.2). We define λ as

$$\lambda = f\lambda_0 = f\frac{M_0\omega}{\hbar} \tag{2.6}$$

and the constant f is chosen such that one obtains a HO spectrum that best fits the discrete part of $V(r)$ (this usually is a realistic Woods-Saxon potential). In Fig. 1 we show schematically the Woods-Saxon potential (dark line) and the HO potential determined by λ (full line).

The solution given by (2.5) is exact if one takes all the terms in the expansion. For spectroscopic calculations (discrete part of the spectrum and transition probabilities) in heavy nuclei it is sufficient to take in the expansion of the radial wave function terms up to $N_0 = 2n_0 + l = 6$ major shells. One thus gets a good description of the wave functions up to the geometrical nuclear radius $R_0 = 1.2A^{1/3}$.

As discussed above, this approach is not enough for a microscopic description of the α or cluster-decay processes, for which it is very important to reproduce the wave function at distances larger than the nuclear radius. It is known that in order to have a proper asymptotic behavior of the wave functions at large distances it is necessary to include up to $N = 18$ major shells in heavy nuclei [16]. But this can also be achieved by using a mixed nonorthogonal HO basis in the diagonalization procedure, thus reducing the number of shells needed in the expansion and, at the same time, obtaining a better description of the decay process. That is, instead of the expansion (2.5) we will use the representation

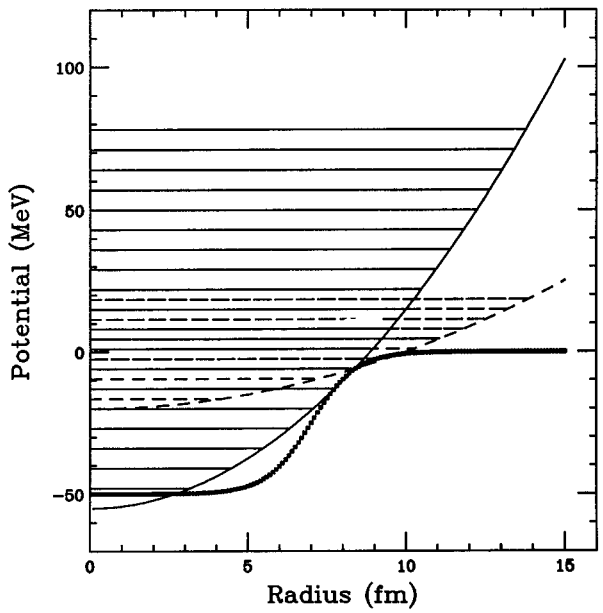

FIG. 1. The harmonic oscillator potentials that define our representation. The full line is the potential that provides the low lying shells of the basis and the dashed line the one that provides the high lying shells. The dark line is the Woods-Saxon potential.

$$u_\alpha(r) = \sum_{2n_1 + l = N_1 \le N_0} c_{\alpha n_1}^{(1)} R_{n_1 l}^{(\lambda_1)}(r) + \sum_{2n_2 + l = N_2 > N_0} c_{\alpha n_2}^{(2)} R_{n_2 l}^{(\lambda_2)}(r) \tag{2.7}$$

where λ_1 is the HO parameter corresponding to the HO potential which fits the Woods-Saxon interaction in the region of the discrete spectrum (the full line of Fig. 1), while λ_2 corresponds to a HO potential that describes better the continuum part of the spectrum (dashed line in Fig. 1). Notice that these two different HO potentials are both centered at the origin of coordinates.

Below we will describe how to evaluate the amplitudes c in Eq. (2.7). But it is worthwhile to point out here that although the representation used in (2.7) is discrete, the density of states is larger at high energies. In fact it can be made as large as one wishes by properly decreasing the parameter λ_2, as indicated in Fig. 1. This is just what is needed to describe processes occurring at distances larger than the nuclear surface.

For each of the HO potentials of Fig. 1 the radial wave function R satisfies

$$H_{lj}^{(\lambda_i)}R_{nl}^{(\lambda_i)}(r) = \hbar\omega\left(2n + l + \frac{3}{2} - \frac{\lambda_i r^2}{2}\right)R_{nl}^{(\lambda_i)}(r) \tag{2.8}$$

where

$$H_{lj}^{(\lambda_i)} = -\frac{\hbar\omega}{2\lambda_i}\left[\frac{1}{r}\frac{d^2}{dr^2}r - \frac{l(l+1)}{r^2}\right]R_{nl}^{(\lambda_i)}(r) \tag{2.9}$$

and λ_i is the HO parameter of the potential i.

The diagonalization of the potential V in terms of the two HO representations can be performed by inserting in Eq. (2.1) the expanded wave function (2.7). One then obtains the following set of equations:

$$\begin{pmatrix} \mathcal{H}^{(11)}_{n_1n_1'} & \mathcal{H}^{(12)}_{n_1n_2'} \\ \mathcal{H}^{(21)}_{n_2n_1'} & \mathcal{H}^{(22)}_{n_2n_2'} \end{pmatrix} \begin{pmatrix} c^{(1)}_{\alpha n_1'} \\ c^{(2)}_{\alpha n_2'} \end{pmatrix} = E \begin{pmatrix} \mathcal{I}^{(11)}_{n_1n_1'} & \mathcal{I}^{(12)}_{n_1n_2'} \\ \mathcal{I}^{(21)}_{n_2n_1'} & \mathcal{I}^{(22)}_{n_2n_2'} \end{pmatrix} \begin{pmatrix} c^{(1)}_{\alpha n_1'} \\ c^{(2)}_{\alpha n_2'} \end{pmatrix} \tag{2.10}$$

where the amplitudes c are as in Eq. (2.7) and the overlap integrals are defined by

$$\mathcal{I}^{(ik)}_{n_in_k'} \equiv \langle \lambda_i n_i l | \lambda_k n_k' l \rangle = \langle R^{(\lambda_i)}_{n_i l} | R^{(\lambda_k)}_{n_k' l} \rangle, \tag{2.11}$$

while the Hamiltonian kernels are given by

$$\mathcal{H}^{(ik)}_{n_in_k'} = \hbar\omega f_k [(2n_k' + l + \tfrac{3}{2}) \mathcal{I}^{(ik)}_{n_in_k'} - \tfrac{1}{2} \langle \lambda_i n_i l | \lambda_k r^2 | \lambda_k n_k' l \rangle] + \langle \lambda_i n_i l | V | \lambda_k n_k' l \rangle \tag{2.12}$$

where, as in Eq. (2.6),

$$f_k = \frac{\lambda_k}{\lambda_0}, \quad k = 1,2. \tag{2.13}$$

The overlap integrals (2.11) can be written in terms of gamma functions [21].

A method to diagonalize the Hermitian system (2.10), corresponding to the representation of the Schrödinger operator in a nonorthogonal basis, is described in the Appendix.

B. Formation amplitude

Let us consider the ground state to ground state α-decay process for an even-even nucleus

$$B \rightarrow A + \alpha. \tag{2.14}$$

We will assume that the mother nucleus (B) and the daughter nucleus (A) are spherically symmetric. Within the R-matrix approach [22,23] the total α-decay width can be written as

$$\Gamma(R) = \sum_{L_\alpha = 0}^{\infty} \gamma^2_{L_\alpha}(R) P_{L_\alpha}(R) \tag{2.15}$$

where the reduced width $\gamma^2_{L_\alpha}(R)$ is proportional to the formation amplitude $F_{L_\alpha}(R)$ squared, i.e.,

$$\gamma^2_{L_\alpha}(R) = \frac{\hbar^2}{2M_\alpha} R |F_{L_\alpha}(R)|^2. \tag{2.16}$$

The L_α component of the formation amplitude is the overlap integral between the entrance and exit α-decay channels, i.e.,

$$F_{L_\alpha}(R) = \int d\hat{R} d\xi_\alpha d\xi_A d\xi_B [Y_{L_\alpha}(\hat{R}) \Psi_\alpha(\xi_\alpha) \Psi_A(\xi_A)]^* \Psi_B(\xi_B) \tag{2.17}$$

where $\hat{R} = (\theta, \phi)$ are the angular center of mass coordinates and $\Psi_X(\xi_X)$ is the internal wave function of the nucleus X with internal coordinates ξ_X.

As usual [24], we write the internal α-particle wave function as a product of $n = l = 0$ HO states, i.e.,

$$\Psi_\alpha(\xi_\alpha) = \Phi^{(\lambda_\alpha)}_{00}(\vec{r}_\pi) \Phi^{(\lambda_\alpha)}_{00}(\vec{r}_\nu) \Phi^{(\lambda_\alpha)}_{00}(\vec{r}_{\pi\nu}) \chi^{(\pi)}_{00}(s_1, s_2) \times \chi^{(\nu)}_{00}(s_3, s_4) \tag{2.18}$$

where Φ is the radial HO wave function with parameter $\lambda_\alpha = 0.513 \text{fm}^{-2}$, [24] χ the corresponding spin wave function, and

$$\vec{r}_\pi = \frac{\vec{r}_1 - \vec{r}_2}{\sqrt{2}}, \quad \vec{r}_\nu = \frac{\vec{r}_3 - \vec{r}_4}{\sqrt{2}}, \quad \vec{r}_{\pi\nu} = \frac{\vec{r}_\pi - \vec{r}_\nu}{\sqrt{2}}, \tag{2.19}$$

where we have labeled by 1,2 the proton and by 3,4 the neutron coordinates.

We will describe the mother and daughter nuclei within the BCS formalism [24]. That is [14],

$$\Psi_X(\xi_X) = \psi_{X\pi}(\xi_\pi) \psi_{X\nu}(\xi_\nu), \quad X = A, B, \tag{2.20}$$

where

$$\psi_{X\tau}(\xi_\tau) = \langle \xi_\tau | \text{BCS} \rangle_{X\tau}, \quad \tau = \pi, \nu. \tag{2.21}$$

One can write the mother nucleus wave function assuming the daughter to be the core. Thus in configuration space one gets, for protons,

$$\psi_{B\pi} = \sum_{\alpha_\pi} \chi_{\alpha_\pi} \sum_{\Omega > 0} \mathcal{A}[\psi_{\alpha_\pi \Omega}(1) \psi_{\alpha_\pi \bar{\Omega}}(2)] \psi_{A\pi}, \tag{2.22}$$

and a similar expression for the neutrons. Here

$$\psi_{\alpha_\pi \bar{\Omega}} = (-)^{j-\Omega} \psi_{\alpha_\pi - \Omega} \tag{2.23}$$

is the time reversed wave function. In the Fock space this corresponds to the expansion

$$|\text{BCS}\rangle_{B\tau} = \sum_{\alpha_\tau} \chi_{\alpha_\tau} \sum_{\Omega > 0} a^\dagger_{\alpha\Omega} a^\dagger_{\alpha\bar{\Omega}} | \text{BCS} \rangle_{A\tau} \tag{2.24}$$

where $a^\dagger_{\alpha_\tau \Omega}$ are the creation operators corresponding to normal particles. The coefficients χ_{α_τ} can be written in terms of the BCS occupation amplitudes as

$$\chi_{\alpha_\tau}={}_{B\tau}\langle \mathrm{BCS}|a^\dagger_{\alpha_\tau\Omega}a^\dagger_{\alpha_\tau\bar{\Omega}}|\mathrm{BCS}\rangle_{A\tau}$$
$$=\frac{U^{(A)}_{\alpha_\tau}V^{(B)}_{\alpha_\tau}}{U^{(A)}_{\alpha_\tau}U^{(B)}_{\alpha_\tau}+V^{(A)}_{\alpha_\tau}V^{(B)}_{\alpha_\tau}}\prod_{\alpha'_\tau}(U^{(A)}_{\alpha'_\tau}U^{(B)}_{\alpha'_\tau}+V^{(A)}_{\alpha'_\tau}V^{(B)}_{\alpha'_\tau})$$
$$\cong U^{(A)}_{\alpha_\tau}V^{(B)}_{\alpha_\tau}. \tag{2.25}$$

By using Eq. (2.7) one obtains for the 2π expansion

$$\psi_{B\pi}=\sum_{\alpha_\pi}\sum_{n_in_k}B_\pi(\alpha_\pi n_in_k)[\phi^{(\lambda_i)}_{n_i(lj)_\pi}(1)\phi^{(\lambda_k)}_{n_k(lj)_\pi}(2)]_0\psi_{A\pi} \tag{2.26}$$

where

$$B_\pi(\alpha_\pi n_in_k)\equiv\frac{\hat{j}}{\sqrt{2}}\chi_{\alpha_\pi}c^{(i)}_{\alpha_\pi n_i}c^{(k)}_{\alpha_\pi n_k}. \tag{2.27}$$

A similar expansion is obtained for the neutron part:

$$\psi_{B\nu}=\sum_{\beta_\nu}\sum_{n'_in'_k}B_\nu(\beta_\nu n'_in'_k)[\phi^{(\lambda'_i)}_{n'_i(lj)_\nu}(3)\phi^{(\lambda'_k)}_{n'_k(lj)_\nu}(4)]_0\psi_{A\nu} \tag{2.28}$$

where

$$B_\nu(\beta_\nu n'_in'_k)\equiv\frac{\hat{j}}{\sqrt{2}}\chi_{\beta_\nu}c^{(i')}_{\beta_\nu n'_i}c^{(k')}_{\beta_\nu n'_k}. \tag{2.29}$$

One can perform all integrals over the integral coordinates in Eq. (2.17) analytically by transforming to relative coordinates. Using the generalized Talmi-Moshinsky transformation with different masses [28] (i.e., with different size parameters λ_1 and λ_2 in our case) one obtains for $L_\alpha=0$

$$F_0(R)=\sum_{Nkik'k'}\Phi^{(\Lambda^{i'k'}_{ik})}_{N0}(R)$$
$$\times\sum_{nN_\pi N_\nu}\langle n0N0;0|N_\pi 0N_\nu 0;0\rangle_{D^{i'k'}_{ik}}$$
$$\times\mathcal{I}^{(\lambda^{i'k'}_{ik},\lambda_\alpha)}_{n0}G^{(ik)}_{N_\pi}G^{(i'k')}_{N_\nu} \tag{2.30}$$

where $G^{(ik)}_\pi$ ($G^{(i'k')}_\nu$) is a geometrical coefficient depending on the proton (neutron) single particle parameters. Thus for the proton it is [14]

$$G^{(ik)}_{N_\pi}=\sum_{\alpha_\pi n_\pi}\sum_{n_in_k}B_\pi(\alpha_\pi n_in_k)$$
$$\times\left\langle(l_\pi l_\pi)0\left(\frac{1}{2}\frac{1}{2}\right)0;0\middle|\left(l_\pi\frac{1}{2}\right)j_\pi\left(l_\pi\frac{1}{2}\right)j_\pi;0\right\rangle$$
$$\times\langle n_\pi 0N_\pi 0;0|n_il_\pi n_kl_\pi;0\rangle_{D_{ik}}\mathcal{I}^{(\lambda_{ik},\lambda_\alpha)}_{n_\pi 0} \tag{2.31}$$

where B_π are the coefficients given by Eq. (2.27). The first angular brackets denote jj-LS recoupling coefficients and the second the generalized Talmi-Moshinsky symbol depending on the ratio $D_{ik}=\lambda_i/\lambda_k$. The quantities $\mathcal{I}^{(\lambda_i,\lambda_\alpha)}_{n_\pi 0}$ are the overlap integrals of Eq. (2.11), which now read

$$\mathcal{I}^{(\lambda_{ik},\lambda_\alpha)}_{n_\pi 0}=\langle R^{(\lambda_{ik})}_{n_\pi 0}|R^{(\lambda_\alpha)}_{00}\rangle \tag{2.32}$$

with the relative HO parameter corresponding to one particle moving in the potential i and the other in the potential k, i.e.,

$$\lambda_{ik}=\frac{\lambda_i\lambda_k}{\Lambda_{ik}}, \tag{2.33}$$

and the corresponding center of mass parameter

$$\Lambda_{ik}=\frac{1}{2}(\lambda_i+\lambda_k). \tag{2.34}$$

The radial c.m. wave function $\Phi^{(\Lambda^{i'k'}_{ik})}_{N_\alpha L_\alpha=0}(R)$ corresponds to a HO potential with the relative and c.m. parameters given by

$$\lambda^{i'k'}_{ik}=\frac{\Lambda_{ik}\Lambda_{i'k'}}{\Lambda^{i'k'}_{ik}}, \tag{2.35}$$

$$\Lambda^{i'k'}_{ik}=\frac{1}{2}(\Lambda_{ik}+\Lambda_{i'k'}). \tag{2.36}$$

The overlap integrals $\mathcal{I}^{\lambda^{i'k'}_{ik}}_{n_\alpha 0}$ are defined in a similar way as above with the generalized Talmi-Moshinsky coefficients depending on the mass ratio

$$D^{i'k'}_{ik}=\Lambda_{i'k'}/\Lambda_{ik}. \tag{2.37}$$

Since in the applications it may be interesting to know in what potential a given particle is moving, we will clearly specify all the possible combinations in the summation (2.30). There are five terms; they are

$$(1)\quad i=k=1,\quad i'=k'=1;$$

$$(2)\quad i=k=2,\quad i'=k'=2;$$

$$(3)\quad i=k=1,\quad i'=k'=2;$$

$$i=k=2,\quad i'=k'=1;$$

$$i\neq k,\quad i'\neq k';$$

$$(4)\quad i=k=1,\quad i'\neq k';$$

$$i\neq k,\quad i'=k'=1;$$

$$(5)\quad i=k=2,\quad i'\neq k';$$

$$i\neq k,\quad i'=k'=2.$$

The formation amplitude can then be written as

$$F_0(R)=\sum_{k=1}^{5}F^{(k)}_0(R). \tag{2.38}$$

We will refer to this summation in the applications below, but from the outset one may expect that properties mainly induced by the motion of the particles inside the nuclear volume will be determined by the term $F_0^{(k=1)}(R)$.

III. NUMERICAL RESULTS

A. Diagonalization procedure

In this section we will apply the method developed above to describe the α decay of ^{220}Ra. This nucleus, as well as the daughter nucleus ^{216}Rn, has a quadrupole deformation $\beta_2 \cong 0.1$. As shown in Ref. [15] for this value of the deformation the inclusion of the nonspherical terms in the estimation of the microscopic formation amplitude changes the final result (total decay width) only by a few percent. It is therefore important to analyze the extent to which a description of this case in terms of a spherical mean field is valid.

For the Woods-Saxon mean field we take the so called universal parametrization [11].

We use the value $N_0=6$ for the principal quantum number defining the limit between the two kinds of terms in the expansion (2.7). We will perform the calculation by using a total of 11 shells. For the HO parameter that is supposed to describe the discrete part of the spectrum we choose the value $f_1=1.2$ [see Eq. (2.6)]. This part of the spectrum should be insensitive to the value of the HO parameter defining the quasicontinuum part, i.e., to f_2. One indeed sees in Fig. 2 that this is the case.

This is an important conclusion because it implies that the orthogonalization procedure, which mixes all states, will not affect the discrete part of the spectrum. That is, one knows well the HO parameters that provide a good representation to describe bound properties in the nucleus. Our procedure, which is intended to allow the calculation of processes in the continuum, increases the dimension of the representation, but without affecting the calculated bound properties.

One also sees in Fig. 2 that the high energy part of the spectrum is strongly dependent upon f_2. For $f_2=f_1=1.2$ the spectrum corresponds to the one used in standard calculations, i.e., by using one HO potential only. As f_2 decreases the level density increases and the representation is, therefore, more suited to describe the quasicontinuum spectrum. That is, by choosing a small HO parameter λ_2 the representation becomes more adequate to describe the wave functions at large distances. But the drawback of using a small value for λ_2 is that the dimension of the representation may become big and the calculation cumbersome, a feature that we want to avoid. That will happen if, e.g., one wants to include all possible shells up to a given energy. Yet one can find a value of f_2 that greatly improves the calculation while the number of shells needed is less than the one used within only one HO potential, as will be shown below.

B. The formation amplitude and total width

The width (2.15) consists of two very distinct parts, namely, the formation probability and the penetration through the Coulomb barrier. Deformations are very important regarding the penetration through the Coulomb barrier, but the formation amplitude corresponding to ground state to ground state decays is not dependent on the deformation parameters [16]. We therefore will calculate in this section the formation amplitude neglecting deformations. The effects of deformations on the penetration will be shown at the end.

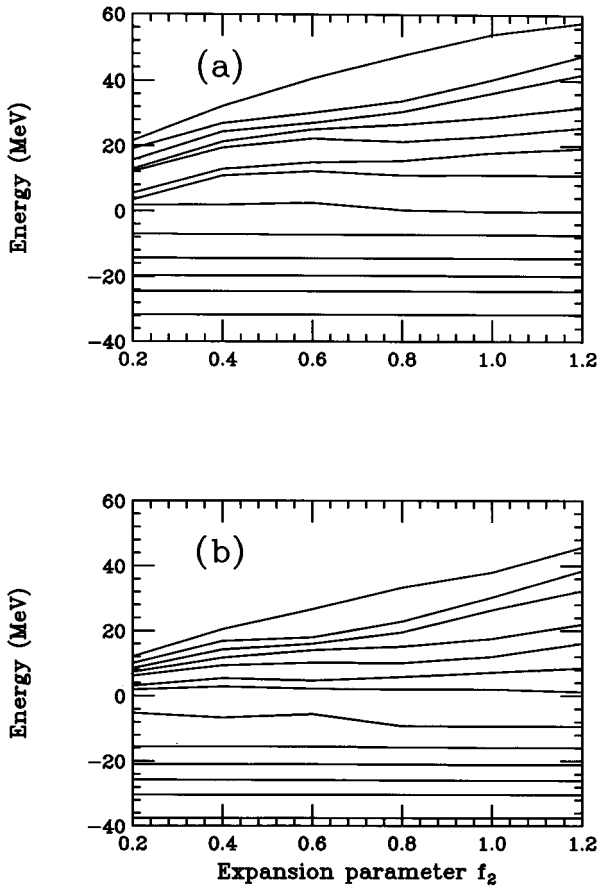

FIG. 2. Single particle levels in ^{220}Ra as a function of the harmonic oscillator parameter f_2 for $f_1=1.2$. The basis consists of the shells $N_1=1-6$ (corresponding to f_1) and $N_2=7-11$ (corresponding to f_2). We call this ''minimal basis.'' (a) Protons, and (b) neutrons.

In order to evaluate the formation amplitude we have first to perform the BCS calculation that defines the intrinsic wave functions of the nuclei involved in the decay. We estimated the BCS parameters by using the third order mass difference relation [29], which gives for ^{220} Ra $\Delta_p=1.091$ MeV, $\Delta_n=0.914$ MeV, and for ^{216} Rn: $\Delta_p=1.066$ MeV, $\Delta_n=0.926$ MeV. We then computed the occupation amplitudes U and V for each system as a function of the parameter f_2.

It is worthwhile to stress here that a large scale shell model calculation would be the best proper way to include a large configuration mixing. Anyway this is almost impossible when many active particles are considered. That is why the BCS method has been widely used since the pioneering work by Soloviev [25] in α-decay calculations. In addition we have shown [26] how the mixing induced by pairing interaction at the level of BCS approximation, for spherical as well as for deformed nuclei, is able to induce a large enhancement of clustering properties in heavy spherical or deformed nuclei. In particular, we have arrived at the con-

clusion that the effective inclusion of the nuclear correlations (particularly the proton-neutron interaction) through the procedure of fitting the strength to reproduce the experimental pairing gap is somehow a proper way of including the very complicated correlations that induce clustering in nuclei [27].

The idea of this calculation was to find a minimal basis that describes well the calculated width. As mentioned above, f_1 was fixed to have the value $f_1=1.2$ and, therefore, the possible different bases are determined by the parameter f_2. But let us stress once more that the results do not (and cannot) depend on the value that one chooses for f_2. If f_2 is big then one needs many shells to reach the final values of the calculated quantities, as expected [16]. We found that the minimal basis is given by the choice $f_2=0.7$. The basis consists then of the HO shells $N_1=0-6$ corresponding to the parameter $f_1=1.2$ and the shells $N_2=7-11$ corresponding to $f_2=0.7$. Considering that the basis provided by only one harmonic oscillator potential requires at least 18 major shells to reproduce the experimental results [16] one can say that our basis is very small.

We performed the calculation within the minimal basis around the touching radius which is defined by

$$R_c=1.2(A_{^{216}\mathrm{Rn}}^{1/3}+A_{^{4}\mathrm{He}}^{1/3})=9.15\ \text{fm}. \tag{3.1}$$

In Fig. 3(a) we present different terms entering the formation amplitude (2.38) as a function of the c.m. radius R. One sees that the contribution corresponding to the discrete part of the spectrum ($k=1$, drawn by dashes) is peaked on the nuclear radius while the mixed contribution between discrete and quasicontinuum parts ($k=3$, plotted by dots) is centered on the touching radius. The total amplitude is drawn by a solid line.

An important test for the calculation is that it should be independent of the distance R outside the nuclear surface. This dependence is shown in Fig. 3(b) for the three cases of Fig. 3(a). One can notice that the main contribution to the total width is provided by the term in Eq. (2.38) that contributes most to the formation amplitude around the touching radius, i.e., the term $k=3$. The contribution from the inner part of the nucleus ($k=1$) is very small. The total contribution (full line) is indeed practically independent of the distance for $R\geqslant 9$ fm, i.e., beyond the touching radii, and reproduces well the experimental value. For smaller radii the width is very small. This is because we have neglected antisymmetrization effects between the daughter nucleus and the α cluster [30–32] but this does not affect our results because we are able to compute the formation amplitude well beyond the touching point, where those effects are negligible [13]. This is the main reason why it is important to have a reliable theory capable of describing the decay process at large distances.

It is interesting to analyze the reason why the minimal basis reproduces so well the experimental data, although it is relatively a very small basis. We thus show in Fig. 4(a) the ratio between the calculated width and the corresponding experimental value as a function of the parameter f_2. One sees that the calculated width reaches the experimental value just in a region of f_2 values around $f_2=0.7$. Outside this

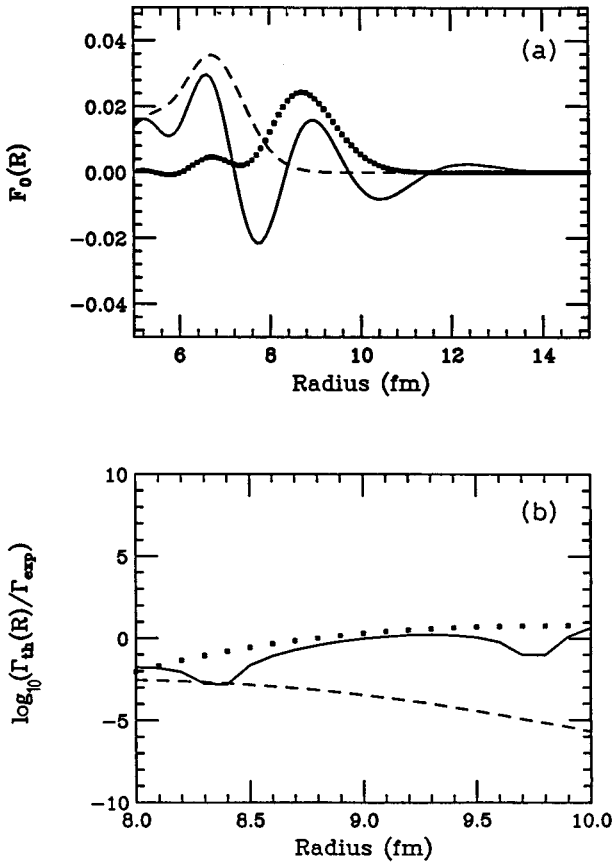

FIG. 3. Formation amplitude (a) and ratio between the theoretical and experimental width (b) corresponding to the ground state to ground state transition of ^{220}Ra as a function of the distance between the α particle and the daughter nucleus ^{216}Rn. The minimal basis was used. The dashed line is the contribution from $F_0^{(k=1)}$ in the expansion (2.38) while the dotted line is the contribution from $F_0^{(k=3)}$. The final values are represented by the full lines.

region the theory does not reproduce the experimental value within the shells included in the minimal basis. That is, outside this region the basis does not span the Hilbert subspace that contains the functions determining the α decay process around the touching radius.

In Fig. 4(b) one sees that increasing the basis dimension one gets saturation.

One also observes in Fig. 4 that the main contribution to the formation amplitude is provided by the term $F_0^{(k=3)}$ in the expansion (2.38) (plotted by dots), while the contribution from the discrete part ($k=1$, plotted by a dashed line) is very small.

One concludes that it is not possible to reproduce the experimental value in a region around the touching point with a smaller number of major shells for any value of the expansion parameter because then the maximum would lie under the experimental value.

Another quantity that can be calculated with our formalism is the spectroscopic factor

$$S=\int_0^\infty |F_0(R)|^2R^2dR. \tag{3.2}$$

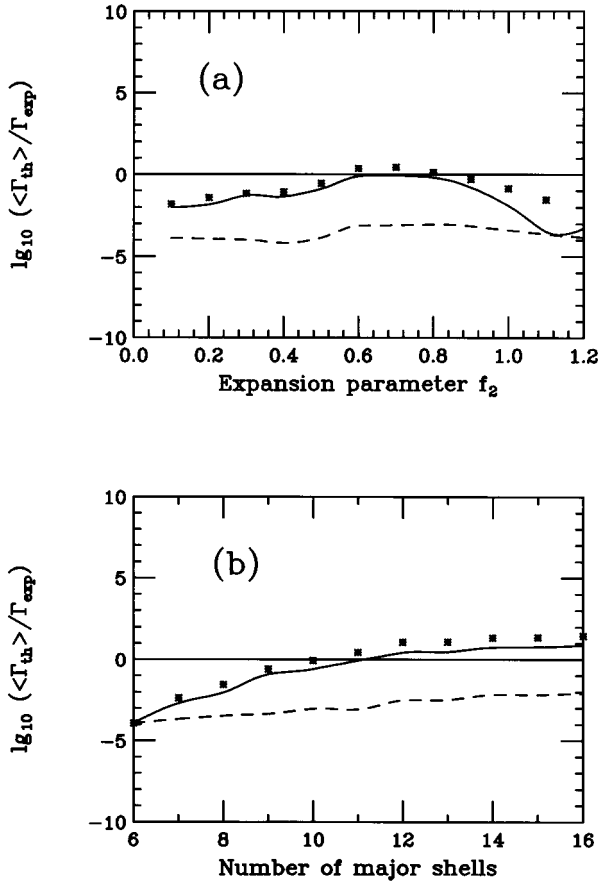

FIG. 4. Ratio between the theoretical and experimental decay widths calculated as in Fig. 3 as a function of (a) the parameter f_2 and (b) the number of shells N_2.

The result of the calculation for this decay is $S=7.0\times10^{-2}$, which is in agreement with a calculation where the Pauli principle acting among the particles in the core and in the α particle was taken into account properly [31].

It is also interesting to analyze the influence of the pairing correlations on the decay process. We found that the calculated results are very sensitive to the BCS parameters, as shown in Fig. 5. In this figure the dependence of the ratio between the calculated and experimental widths as a function of the gap parameter is presented (full line). One sees that the total width can change by several orders of magnitude by changing Δ within ''reasonable'' limits. It is thus remarkable that choosing the Δ value prescribed by spectroscopic calculations in agreement with experimental data one gets just the right width.

The calculation of the formation amplitude was performed by neglecting deformations. These are only important regarding the penetration through the Coulomb barrier. This is also shown in Fig. 5 (dashed line), where one sees that the calculated decay width, for a quadrupole deformation $\beta_2=0.3$, increases by a factor of 5, practically independently of the BCS parameters. Again in this case, it is remarkable that one gets the experimental width by just taking the deformation parameters extracted from spectroscopic studies.

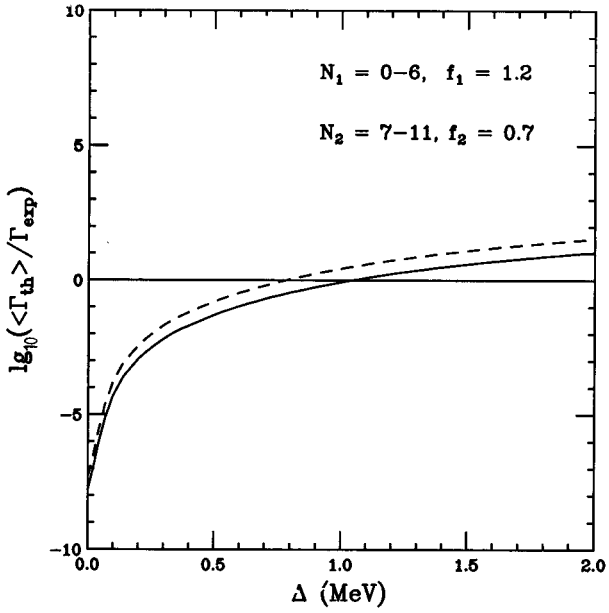

FIG. 5. Dependence of the averaged width on the BCS gap parameter corresponding to a spherical barrier (solid line) and a deformed barrier (dashed line) for the ground state to ground state decay of ^{220}Ra.

C. α decay systematics

In this section we will analyze ground state to ground state α decays from even-even nuclei by using the minimal basis discussed in the previous section, i.e., by choosing the HO shells according to

$$f_1=1.2, \quad N_1=0-6; \quad f_2=0.7, \quad N_2=6-11. \quad (3.3)$$

For the Woods-Saxon potential we adopted again the universal set of values [11]. As in the previous section, the BCS gap parameters were calculated according to the third order mass formula [29]. Even if the dependence of the width upon the distance around the touching point is weak, we will present the calculated values averaged on the interval $R=8-10$ fm, i.e., around the touching point.

We have calculated the total α-decay width corresponding to 26 cases of even-even heavy nuclei, i.e., above ^{208}Pb in the periodic table. The aim of this calculation is to probe the validity of the conclusions reached in the previous section for a large number of nuclei as well as to analyze the effect of deformations on the decay process. For this we computed the total width by using a spherical as well as a deformed Coulomb barrier for the penetration problem. In both cases we applied the semiclassical (WKB) approximation, which is known to be very good in α decay [15,33]. The deformation parameters were taken from Ref. [35] and the experimental values of the widths from Refs. [19,34].

In Table I are given the results of the calculation. Considering that this is a complete microscopic calculation without any free parameter, one can say that the agreement between theory and experiment is excellent.

One important feature that can be seen in this table is the contributions of deformations to the decay widths. As expected, when the deformation increases the difference be-

TABLE I. Absolute α-decay widths calculated assuming a spherical barrier (Γ_{sph}) and deformed barrier defined by the parameter β_2 (Γ_{exp}). The calculation was performed within the minimal basis. The deformation parameters are from Ref. [35] and the experimental values of the widths from Refs. [34,19]. The Fröman method [33] has been used to calculate the penetration through the deformed Coulomb barrier.

No.	Nucleus	β_2	Γ_{exp} (MeV)	Γ_{sph} (MeV)	Γ_{def} (MeV)	$\Gamma_{sph}/\Gamma_{exp}$	$\Gamma_{def}/\Gamma_{exp}$
1	^{212}Po	0.00	1.5(-15)	1.7(-15)	1.7(-15)	1.14	1.14
2	^{214}Po	0.00	2.9(-18)	1.5(-18)	1.5(-18)	0.53	0.53
3	^{216}Po	0.00	3.0(-21)	2.0(-21)	2.0(-21)	0.68	0.68
4	^{218}Po	0.00	2.4(-24)	1.3(-24)	1.3(-24)	0.56	0.56
5	^{216}Rn	0.07	1.0(-17)	4.8(-18)	5.0(-18)	0.47	0.50
6	^{218}Rn	0.09	1.3(-20)	6.7(-21)	7.3(-21)	0.51	0.56
7	^{220}Rn	0.13	8.1(-24)	4.5(-24)	5.6(-24)	0.55	0.69
8	^{222}Rn	0.14	1.4(-27)	6.1(-28)	8.3(-28)	0.44	0.60
9	^{220}Ra	0.11	2.0(-20)	1.5(-20)	1.8(-20)	0.79	0.91
10	^{222}Ra	0.19	1.2(-23)	5.4(-24)	9.1(-24)	0.46	0.77
11	^{224}Ra	0.18	1.4(-27)	5.2(-28)	8.4(-28)	0.37	0.61
12	^{226}Ra	0.20	8.6(-33)	2.6(-33)	5.0(-33)	0.30	0.58
13	^{224}Th	0.21	3.5(-22)	1.4(-22)	2.5(-22)	0.39	0.71
14	^{226}Th	0.23	1.8(-25)	4.7(-26)	1.0(-25)	0.26	0.56
15	^{228}Th	0.23	5.5(-30)	1.7(-30)	3.9(-30)	0.30	0.71
16	^{230}Th	0.24	1.5(-34)	5.0(-35)	1.4(-34)	0.34	0.94
17	^{232}Th	0.26	8.0(-40)	2.2(-40)	7.6(-40)	0.27	0.94
18	^{230}U	0.26	1.7(-28)	7.1(-29)	2.1(-28)	0.42	1.24
19	^{232}U	0.26	1.4(-31)	4.6(-32)	1.5(-31)	0.32	1.04
20	^{234}U	0.27	4.2(-35)	1.1(-35)	4.0(-35)	0.26	0.96
21	^{236}U	0.28	4.6(-37)	9.8(-38)	4.1(-37)	0.22	0.89
22	^{238}U	0.28	2.5(-39)	3.7(-40)	1.6(-39)	0.14	0.65
23	^{238}Pu	0.28	1.2(-31)	3.5(-32)	1.4(-31)	0.30	1.21
24	^{240}Pu	0.29	1.6(-33)	3.1(-34)	1.3(-33)	0.19	0.82
25	^{242}Pu	0.29	3.0(-35)	5.4(-36)	2.5(-35)	0.18	0.82
26	^{244}Pu	0.29	1.4(-37)	2.9(-38)	1.4(-37)	0.20	0.97

tween the calculated spherical and deformed widths also increases, but the contribution of deformations always improves the calculation, sometimes by large factors, as in the decay of ^{244}Pu.

The effects of deformations shown in Table I can perhaps better be seen in Fig. 6, where the ratio between theoretical and experimental widths is presented for the different nuclei of Table I. Open circles correspond to calculations performed within a spherical framework while the stars are the values calculated with deformations. One again sees in this figure that the agreement between theory and experiment is excellent if all the ingredients, including deformations, are properly included in the calculation. The mean value of the ratio between the theoretical and experimental widths is 0.79, with a standard deviation of 0.21. For comparison, one can mention that neglecting deformations (i.e., the ''spherical'' values in Table I) the average value of the ratio is 0.41 with the same standard deviation, i.e., 0.21.

The good agreement between theory and experiment shown in Table I and Fig. 6 has to be consider in the context not only of the dependence of the width upon deformations (shown there) but also of its strong dependence upon the Q value [24] and the BCS parameters, as seen in Fig. 5. All these quantities can be very different in the rather disparate collection of nuclei of Table I.

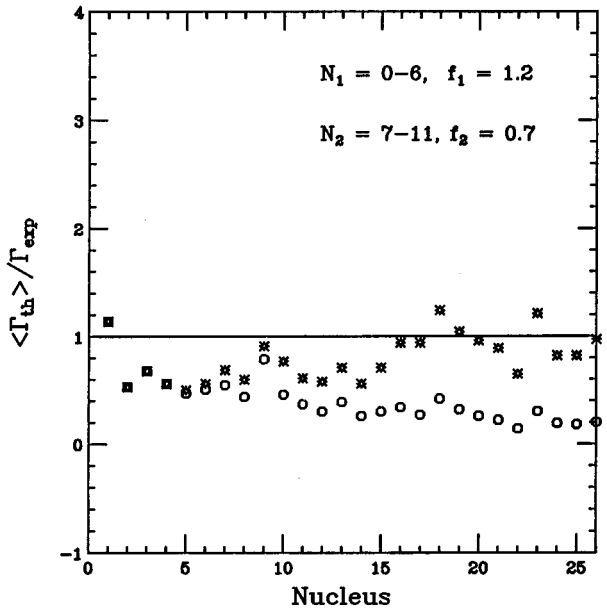

FIG. 6. Ratio between the theoretical and experimental decay widths for spherical (circles) and deformed (stars) barriers corresponding to the decays in Table I. The parameters N and f defining the minimal basis are also given.

IV. CONCLUSIONS

The calculation of absolute α-decay widths is a very difficult undertaking because either one calculates it at a short distance, as for spectroscopic quantities, where the Pauli principle acting among the particles in the core and in the α particle is important, or one calculates it at large distances, where standard shell model representations are inadequate to describe the decay process. In this paper we have attacked this problem by choosing as representation a basis provided by two different harmonic oscillator potentials. The lowest shells of the representation are taken from a HO potential that describes well spectroscopic properties, i.e., distances up to around the nuclear surface. This is the HO potential used generally in spectroscopic calculations, i.e., the one that fits best the corresponding Woods-Saxon potential (see Fig. 1). The highest shells are taken from a HO potential that is rather shallow, thus with a greater density of states in the quasicontinuum, i.e., suited to describe distances outside the nuclear surface. The corresponding basis is formed by the shells $N_1=0-6$ obtained from the HO potential with parameter $f_1=1.2$ [see Eq. (2.13)] and the shells $N_2=7-11$ obtained from the HO potential with $f_2=0.7$. In other words, one can conclude that we have used a realistic single particle basis. The good asymptotic behavior of the single particle wave function means a nonexponential decrease in the tail (for radial distances larger than the nuclear radius). The location of the last maximum for the single particle radial wave function is found at a point where

$$N\hbar\omega = V(r) \tag{4.1}$$

so that if the HO parameter λ is smaller this radius is pushed far away. If this is the case, the previous equation is satisfied for a larger radius and smaller N for a shallower HO potential. The coherent superposition coming from the large mixing of different contributions in the region behind the last maximum produces a non exponential decay of the final α formation amplitude [1,15].

Within this representation one is able to calculate the formation amplitude of the α particle at large distances, thus avoiding the formidable task of considering exactly the Pauli principle between the core and the α particle. In addition, one achieves this with a rather small basis, since it is just constructed to fit the decay process. This basis is nonorthogonal, but one can use any of the methods available to treat such a basis. One of such methods, which is the one used in this paper, is presented in the Appendix.

In our calculations we have used for the mean field standard Woods-Saxon potentials with parameters that we have taken from independent spectroscopic calculations. We included the pairing correlations among the particles as prescribed by standard BCS calculations and, therefore, there is no free parameter in the calculated absolute decay widths.

With these prescriptions we calculated a rather large number of α-decay widths in heavy nuclei. To probe the validity of the calculations, we have checked in all cases that the widths are only weakly dependent upon the distances between the cores and the α particles outside the nuclear surfaces, which in the calculated nuclei are between 8 fm and 10 fm. The calculated values of the widths agree well with the corresponding experimental values. The mean value of the ratio between the theoretical and experimental decay widths for all calculated cases is 0.79 with a standard deviation of 0.21.

We also calculated spectroscopic factors, which are in good agreement with other calculations, where the Pauli principle was taken into account properly [31]. In this context, it is important to notice that the basis used in this paper (11 major HO shells) is rather small. For comparison one may mention that similar calculations using only one HO potential required the inclusion of 18 major shells [16]. This small basis may make microscopic calculations of more complicated decays (such as the decay of heavy clusters) feasible.

We found that the main contribution to the total width is provided by that part of the formation amplitude centered around the touching point, i.e., the term connecting the discrete and quasicontinuum parts of the single particle spectrum. We also found that deformations are important to describe the decay process properly.

APPENDIX: DIAGONALIZATION PROCEDURE IN A NONORTHOGONAL BASIS

In this appendix we will recall the method to solve the eigenvalue problem for a Hermitian matrix in a nonorthogonal basis (2.10). Let us consider the general eigenvalue problem

$$H\Psi_k = E_k\Psi_k \tag{A1}$$

where the eigenfunction Ψ_k, corresponding to the eigenvalue E_k, is expanded in a nonorthogonal basis ϕ_n,

$$\Psi_k = \sum_n C^T_{kn}\phi_n = \sum_n C_{nk}\phi_n, \tag{A2}$$

T denoting the matrix transposition. Inserting (A2) into Eq. (A1), multiplying to the left by ϕ_m, and integrating one obtains

$$\sum_n \langle\phi_m|H|\phi_n\rangle C^T_{kn} = E_k\sum_n C^T_{kn}\langle\phi_m|\phi_n\rangle. \tag{A3}$$

This is just the general eigenvalue problem to be solved given by Eq. (2.10), with the metric matrix

$$I_{mn} \equiv \langle\phi_m|\phi_n\rangle. \tag{A4}$$

Let us first find the eigenvalues F_j and eigenvectors Y_{lj} of the symmetric metric matrix

$$\sum_l I_{ml}Y_{lj} = F_jY_{mj} \tag{A5}$$

where the orthonormality conditions for the eigenvectors hold:

$$\sum_i Y_{mi}Y^T_{in} = \delta_{mn}. \tag{A6}$$

The system of functions

$$\psi_i = \sum_k \frac{Y^T_{ik}}{\sqrt{F_i}} \phi_k \tag{A7}$$

is orthonormal, because from (A5) and (A6) one obtains

$$\langle \psi_i | \psi_j \rangle = \sum_k \frac{Y^T_{jk}}{\sqrt{F_i}} \sum_l I_{kl} \frac{Y_{lj}}{\sqrt{F_j}} = \sum_k \frac{Y^T_{ik}}{\sqrt{F_i}} \sqrt{F_j} Y_{kj} = \delta_{ij} . \tag{A8}$$

Expanding the initial eigenfunctions Ψ_k (A2) in terms of this basis,

$$\Psi_k = \sum_i X^T_{ki} \psi_i , \tag{A9}$$

one obtains an eigenvalue problem

$$\sum_i \langle \psi_l | H | \psi_i \rangle X^T_{ki} = E_k X^T_{ki} \tag{A10}$$

for the symmetric matrix

$$\langle \psi_l | H | \psi_i \rangle = \sum_{mn} \frac{Y^T_{lm}}{\sqrt{F_l}} \langle \phi_m | H | \phi_n \rangle \frac{Y_{ni}}{\sqrt{F_i}} . \tag{A10}$$

Using (A7) and (A9) one finally obtains the following expression for the expansion coefficients in (A2):

$$C^T_{kn} = \sum_i X^T_{ki} \frac{1}{\sqrt{F_i}} Y^T_{in} . \tag{A11}$$

Here the eigenvalues F_i and the eigenvectors Y^T_{in} are solutions of the system (A5) and (A6) and the eigenvectors X^T_{ki} the solutions of (A10) and (A11).

[1] A. Arima and I. Tonozuka, Nucl. Phys. **A323**, 45 (1979).
[2] G. Dodig-Crnkovic, F. A. Janouch, and R. J. Liotta, Phys. Scr. **37**, 523 (1988); Nucl. Phys. **A501**, 533 (1989).
[3] A. Insolia, R. J. Liotta, and E. Maglione, Europhys. Lett. **7**, 209 (1988).
[4] F. A. Janouch and R. Liotta, Phys. Rev. C **27**, 896 (1983).
[5] R. H. Lemmer and A. E. Green, Phys. Rev. **119**, 1043 (1960).
[6] A. Faessler and R. Sheline, Phys. Rev. **148**, 1003 (1966).
[7] P. Röper, Z. Phys. **195**, 316 (1966).
[8] E. Rost, Phys. Rev. **154**, 994 (1967).
[9] V. V. Paskevitsch and V. M. Strutinsky, Yad. Fiz. **9**, 56 (1969) [Sov. J. Nucl. Phys. **9**, 35 (1969)].
[10] J. Dudek, A. Majhofer, J. Skalski, T. Werner, S. Cwiok, and W. Nazarewicz, J. Phys. G **5**, 1359 (1979).
[11] S. Cwiok, J. Dudek, W. Nazarewicz, J. Skalski, and T. Werner, Comput. Phys. Commun. **46**, 379 (1987).
[12] R. Bengtsson, J. Dudek, W. Nazarewicz, and P. Olanders, Phys. Scr. **39**, 196 (1989).
[13] K. Varga, R. G. Lovas, and R. J. Liotta, Nucl. Phys. **A550**, 421 (1992).
[14] A. Insolia, P. Curutchet, R. J. Liotta, and D. S. Delion, Phys. Rev. C **44**, 545 (1991).
[15] D. S. Delion, A. Insolia, and R. J. Liotta, Phys. Rev. C **46**, 884 (1992); Phys. Rev **46**, 1346 (1992).
[16] D. S. Delion, A. Insolia, and R. J. Liotta, J. Phys. G **19**, L189 (1993); **20**, 1483 (1994).
[17] A. Florescu and A. Insolia, Phys. Rev. C **52**, 726 (1995).
[18] K. Varga and R. J. Liotta, Phys. Rev C **50**, R1292 (1994).
[19] B. Buck, A. C. Merchand, and S. M. Perez, At. Data Nucl. Data Tables **54**, 53 (1993).
[20] I. S. Grant *et al.*, Proposal to the ISOLDE committee, CERN/ISC 94-8, 1994, P61.
[21] J. M. Eisenberg and W. Greiner, *Nuclear Theory I, Nuclear Models* (North-Holland, Amsterdam, 1970).
[22] R. G. Thomas, Prog. Theor. Phys. **12**, 253 (1954).
[23] A. M. Lane and R. G. Thomas, Rev. Mod. Phys. **30**, 257 (1958).
[24] H. J. Mang, Annu. Rev. Nucl. Sci. **14**, 1 (1964); H. J. Mang and J. O. Rasmussen, Dank. Vidensk. Selsk. Mat. Fys. Skr. **2**, No. 3 (1962); J. K. Poggenburg, H. J. Mang, and J. O. Rasmussen, Phys. Rev. **181**, 1697 (1969).
[25] V. G. Soloviev, Phys. Lett. **1**, 202 (1962).
[26] F. Catara, A. Insolia, E. Maglione, and A. Vitturi, Phys. Rev. C **29**, 1091 (1984); Phys. Lett. **149B**, 41 (1984).
[27] We would like to point out here that this has been greatly clarified in an as yet unpublished review paper by R. Lovas *et al.*
[28] M. Sotona and M. Gmitro, Comput. Phys. Commun. **3**, 53 (1972).
[29] A. Bohr and Mottelson, *Nuclear Structure* (Benjamin, New York, 1975), Vol. 1.
[30] T. Fliessbach, H. J. Mang, and J. O. Rasmussen, Phys. Rev. C **13**, 1318 (1976).
[31] R. Blendowske, T. Fliessbach, and H. Walliser, Nucl. Phys. **A464**, 757 (1987).
[32] D. F. Jackson and M. Rhoades-Brown, J. Phys. G **4**, 1441 (1978).
[33] P. O. Fröman, K. Dan. Vidensk. Selsk. Mat. Fys. Skr. **1**, No. 3 (1957).
[34] *Table of Isotopes*, edited by C. M. Lederer and V. S. Shirley (Wiley-Interscience, New York, 1978).
[35] S. Raman, C. H. Malarkey, W. T. Milner, C. W. Nestor, Jr., and P. H. Stelton, At. Data Nucl. Data Tables **36**, 1 (1987).